JOURNAL OF SPACECRAFT AND ROCKETS
Vol. 30, No. 4, July–August 1993

Infrared Thermographic Techniques for Arc-Jet Testing

Susan M. White*
NASA Ames Research Center, Moffett Field, California 94035
and
Douglas Burleigh†
General Dynamics, San Diego, California 92186

Thermography can be used to image materials in the infrared range and to produce two-dimensional maps of surface temperatures of materials in extreme environments and under harsh experimental conditions where directly measuring the surface temperature with probes at all desired locations is either difficult or impossible. Thermography is a process for measuring the surface radiant energy and reducing it to a temperature map of the surface. Until recently quantitative temperature data for arc-jet tests were not easily achievable by thermographic techniques. To obtain quantifiable results, experimenters need reliable effective values for the emittance of the radiating surface, the transmittance of any intervening windows or other media, and the bandpass of any filters. In a new approach, these properties were lumped together and evaluated by integrating the relevant temperature-dependent spectral properties and using the experimental data from a limited set of surface thermocouples. This approach was validated by the good agreement between different surface thermocouples and temperatures derived from thermographic measurements. Thermographic monitoring of a series of arc-jet tests is described. The thermographic data gathered are used to evaluate the heating distribution across the surface of the test model as well as the effect of steps in the model surface on the surface temperature.

Nomenclature

e = emissive power, W/ m^2 μm
$F\epsilon\tau$ = lumped effective optical property
T = temperature, K
Δx = step height between tiles , mm
ϵ = emittance
λ = wavelength, μm
τ = transmittance

Subscripts

C = center surface
TC = thermocouple
TGY = thermography
w = window
λT = at wavelength λ and temperature T

Introduction

THERMOGRAPHY has been used to monitor hypersonic flow tests in the past by Compton[1] of NASA Ames Research Center and by a number of researchers from other institutions, including Boylan et al.,[2] Bandettini and Peake,[3] Carlomagno et al.,[4] Monti and Zuppardi,[5] Simeonides et al.,[6] and Balageas et al.[7] The recent advances in thermography, as discussed by Carlomagno and DeLuca[8] and Henckels and Maurer,[9] have only begun to be fully exploited. Augmenting thermocouple and spot radiometer data with thermography was found to be a valuable tool for a number of other different applications as well.

Presented as Paper 91-0696 at the AIAA 29th Aerospace Sciences Meeting, Reno, NV, Jan. 7–10, 1991; received May 27, 1992; revision received Aug. 24, 1992; accepted for publication Sept. 4, 1992.

*Research Scientist, Thermal Protection Materials Branch, Mail Stop 234-1.

†Senior Physicist, Space Systems Division, P.O. Box 85990, Mail Zone 23-8560.

Heatshield design for advanced space vehicles requires an array of different thermal protection materials, to withstand the wide range of predicted heating environments. The predominant thermal protection material used on the Space Shuttle Orbiter is a tile system composed of rigid fibrous ceramic tiles that are coated with a high-emittance reaction-cured glass (RCG) coating. In this study, a series of thermographically monitored arc-jet tests was performed on an experimental tile model using the 20 MW panel test facility at NASA Ames Research Center. The tile model experimentally simulates a heatshield design.

The individual tiles can be positioned in a staggered pattern over the surface of the vehicle in order to misalign the narrow gaps between the tiles and, in certain designs, to align them at an angle to the streamlines of the air flow over the surface. The surface of the experimental model, like the tiled surface of a vehicle itself, is not aerodynamically smooth but includes surface irregularities such as steps and gaps between tiles. The surface steps result from three different causes: thermal distortion of the tile materials during the firing process, installation of the tiles within the assigned step-height tolerances, and movement during flight. The locations of these steps cannot be predicted and therefore cannot normally be instrumented. The presence of forward-facing steps, in conjunction with other flow and geometric effects, can cause severe local overheating of the materials under conditions that have been characterized by Hube[10] for the Space Shuttle as well as by Neiland[11] for the Buran flight regime, to cite only two references from the extensive literature on this topic. For any new flight regime, the conditions under which overheating can occur needs to be determined as accurately as possible to establish the appropriate step-height tolerances for these new flight conditions. It is therefore necessary to characterize the temperature distribution at stepped locations on a model surface under controlled laboratory conditions to extrapolate the experimental data to new flight regimes that cannot be adequately simulated in ground-based test facilities.

For this work, test conditions were chosen that covered a range of surface heat fluxes from 7.4 to 34.6 W/cm^2. Experimental runs were made imposing both step heat pulses and simulated trajectories to yield sufficient data for analysis. Both the angle of attack of the model and the arc-jet operating conditions were changed during the tests to control the heat flux to the surface of the model. Figure 1 shows the imposed surface heat flux vs time for one of the tests. A series of eight arc-jet tests was thermographically moni-

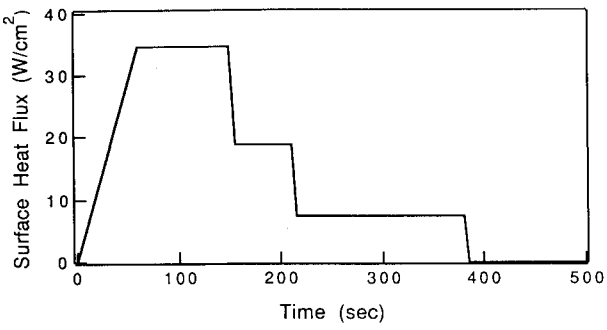

Fig. 1 Imposed heat flux on the surface of the model during arc-jet test.

tored. Each test was monitored from the time the arc was established through the heating and cooling phases of the model. The thermographic data were recorded on videotape and postprocessed by computer.

Temperature Measurement Techniques

Subsurface temperatures in the majority of tile test models are easily measured with thermocouples; however, the surface temperatures are generally of the greatest interest. Frequently the surface temperatures can be difficult to measure with thermocouples (TCs) or resistance thermometric devices (RTDs) because the surface itself is a thin coating or a porous layer. The sensor must be in good thermal contact with the surface but not protrude through it. The lead wire must be small gauge, must have small junctions, and must be installed from the rear of the test specimen. Generally, to instrument a tile, a hole is bored through the substrate to the surface and the thermocouple is inserted before the tile is coated and fired. This is usually difficult, tedious, expensive, and occasionally results in damage to the coating or other parts of delicate models. Thermocouples may not generally be surface mounted, since they can perturb the gas flow over the surface or undergo catalytic reactions with the gas species. To instrument porous models, sensors are mounted directly behind the surface. In both cases, a metallic thermocouple can change the temperature being measured because of thermal conduction, catalysis, heat capacity, or differences between the emittance of the thermocouple and the surrounding material.

Thermocouples are also, of course, limited by their maximum and minimum use temperatures. Type R (Pt-Pt/13% Rh) thermocouples can be used only to 1750 K, whereas several types of tungsten-tungsten rhenium thermocouples can be used to 2600 K, but the chemical reactivity and brittleness of tungsten can cause difficulties. In addition, thermocouples give only point measurements, so where temperature gradients are anticipated, a large number of thermocouples may be required to obtain the desired resolution. Similar restrictions apply to RTDs.

Thermography is a process whereby the surface temperatures are deduced from the infrared energy emitted by a target or source. Generally, this is done by scanning the target with an electromechanical mirror or rotating prism system and converting the incoming radiation to an electrical signal by use of an infrared detector or array of detectors, usually HgCdTe, InSb, PtSi, or others. The electrical signals are then converted to temperature by computations, which depend on several variables, including surface emittance and transmittance of the windows and the lenses in the optical path.

Full field imaging, coupled with high spatial resolution, provided by 50,000 pixels (250×200) or more, provides previously unavailable data on the effects of turbulent flow and localized heating or cooling. Infrared spot radiometers are used to measure or verify temperatures, but these are limited by being local spot measurements. As a means of measuring surface temperature, thermography offers advantages over the use of thermocouples, RTDs, and spot radiometers, because thermography measures surface temperatures, as opposed to point temperatures, by remote noncontact means under conditions where the direct measurement of temperature is difficult or impossible. For example, without thermography it is difficult to measure surface temperatures when temperature gradients are present across the surface, in the presence of irregular surfaces, or under flow conditions imposing a varied surface heat flux boundary condition across the surface. In addition, it is challenging to instrument highly porous materials such as flexible ceramic blanket materials, which are used as reusable re-entry insulation. It is feasible, however, to measure the surface temperatures on these and other complex structures by thermographic means.

Thermographic data are collected at television frame rates, either 20 or 30 Hz. In the cases where this is not sufficiently fast, thermographic line scanning at rates up to 8 kHz can be achieved by locking the vertical scan mechanism. Thermography displays the measurements in a convenient graphical format that can be recorded on videotape. Data can be presented in false color, which is frequently advantageous to interpretation of test results. The infrared system used in the present experiment resolves 256 separate levels of radiance using a grey scale, which is divided over the range of surface temperature variation, typically 100–500 K. The images can also be displayed with a palette of 16 or more colors for ease of interpretation.

The inversion of raw thermographic data to yield accurate temperature data is not always straightforward, however, because the accuracy of thermographic temperature measurements is strongly dependent on the accuracy with which the emittance of the target and the transmittance of the optical path between the scanner and target are known. When the optical path is short and atmospheric absorption is negligible, the only transmissive losses occur in the viewing window and the aluminum mirror on the arc-jet tunnel, both of which can be measured. These transmissive losses vary with wavelength, angle, and temperature. This is discussed in greater detail later.

Under other experimental test conditions than those described here, the following two additional sources of error may become significant. The emittance may change during the test due to ablation, chemical reaction, or phase change at the surface under observation. Any uncharacterized change in emittance will directly result in an erroneous surface temperature when using thermography, unless the thermographic measurements are calibrated against independently measured temperatures. This may be accomplished by the methods described in this paper. In addition, problems could arise from detecting reflections of the electric arc from the target surface. This reflected thermal energy would be interpreted by the infrared camera as having been emitted by the target and would result in an apparent higher surface temperature.

Ideally, we should know the emittance of all of the materials to be tested as a function of both wavelength and angle and all of this as a function of temperature. These data are rare and not easily measured at the high temperatures produced in arc-jet tests. However, the appropriate values for the effective emittance and window transmittance have been calculated in this work from laboratory measurements and correlation with independent surface temperature measurements using thermocouples.

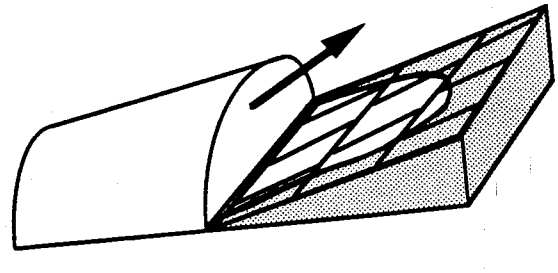

Fig. 2 Sketch of test model showing unshaded region imaged by camera.

Table 2 Effective radiative properties including filter calibration and temperature effects for the three different filters used

Bandpass filter, μm	Blackbody calibrated	Lumped effective radiative property, $F\epsilon\tau$
8–12	Yes	0.90−0.63* (T-730)/1000±0.01
3–5	No	0.70−0.123* (T/1000)±0.02
10.6	No	0.45±0.02

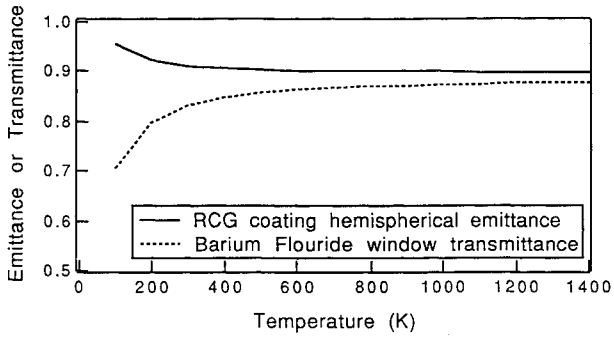

Fig. 3 Effective RCG hemispherical emittance and barium flouride window transmittance for 8-12 μm bandpass filter.

Testing

The experimental model used in these runs was a 47×47 cm panel with 13 removable tiles. Figure 2 is a sketch of the model used in the arc-jet test section. The unshaded area indicates the region typically imaged by the camera. The image is elliptical because the model surface was at an angle to the horizontal. The image of the ellipse is truncated where it intersects with the nozzle. The lines on the model surface show where the gaps are located between the tiles of the model surface. The panel was mounted on a fixture whose angle of attack with respect to the freestream flow was varied from 0 to 8 deg. Six of the tiles in the test model were heavily instrumented with type R (Pt/Pt-13% Rh) thermocouples. The thermocouples measured temperatures on the tile surface, within the tiles, and along the tile gaps. The surface thermocouples are in contact with the coating.

The tiles were composed of a rigid fibrous ceramic material coated with a high-emittance RCG coating. The tile geometry was representative of the tiles on one region of a proposed flight vehicle. The tiles were 2.26 cm thick and were 15.7×13.8 cm parallelograms, with the longer side at 18 deg to the perpendicular. On the flight vehicle, a typical tile will have two edges at 18 deg to the streamline and two edges normal to the streamline. Gaps left between the tiles were typically 0.15–0.25 cm wide, with an average width of 0.20 cm. On a flight vehicle, gaps between tiles are used to compensate for tile motion during flight due to thermal expansion and contraction or vibration.

The thermographic equipment used was an Inframetrics 600 broadband scanner capable of detecting radiant energy over the 3–14 μm infrared wavelength band. It is equipped with wide bandpass filters of 3–5 and 8–12 μm and with narrow bandpass filters of 4.1 and 10.6 μm. It was calibrated by the manufacturer for measuring temperatures to 1800 K. However, calibrations performed at NASA Ames Research Center extended this calibration range to nearly 2300 K.

The scanning camera was mounted on the top of the tunnel. The optical path length from the camera to the test model surface was 1 m. A polished aluminum plate, mounted at a 45-deg angle, was used as a mirror so the camera could be horizontal while looking down into the chamber. For part of the test series, a wide-angle lens was used since it afforded a view of the largest area of the test model, although this reduced the spatial resolution. For the other tests, the standard lens with a variable focal length was used to afford higher spatial resolution of the instrumented center tiles of the experimental model. The spatial resolution of the test setup was 0.023×0.023 m for the wide-angle lens and 0.009×0.009 m for the standard lens.

The windows in the optical path were barium fluoride. The transmittance of barium fluoride was high and constant from below 1 μm to up to nearly 10 μm but fell off rapidly above 10 μm. No alternative to barium fluoride was readily available. A zinc selenide window would have been preferable in the 8–12 μm range for its superior transmittance above 10 μm.

Effective Thermographic Radiative Properties

Extensive measurements have been made of the high-temperature radiative properties of the RCG coating of the tiles, but the available data are not applicable to this analysis since they were not taken over the specific wavelength band used here. The surface emittance required for thermographic use is an effective value of the emittance. When the 8–12 μm filter is in place, it depends only on spectral data between 8–12 μm for the given temperature range. To convert the measured surface radiant energy to surface temperatures, it is necessary to develop single values for the effective surface emittance and the window transmittance in the 8–12 μm range at high temperature. The hemispherical total emittance of the

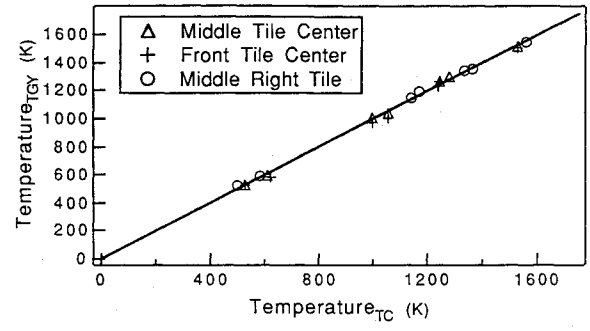

Fig. 4 Comparison of surface thermocouple measurements with thermographic temperature at the surface thermocouple locations shown in boxes in Figs. 7–12.

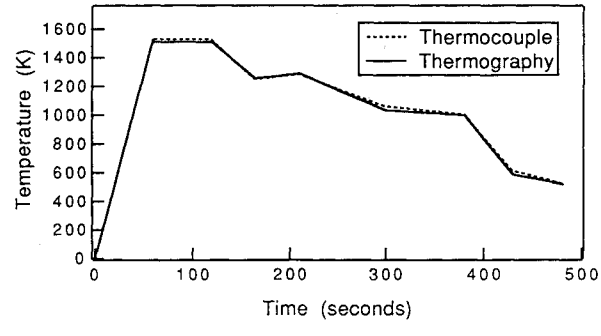

Fig. 5 Comparison of surface thermocouple measurements with thermographic temperature during a typical test.

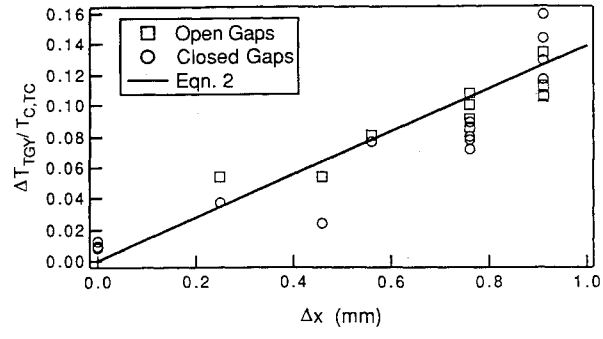

Fig. 6 Step-induced heating of the tile leading edge as a function of step height.

reaction-cured glass surface and the transmittance of the barium fluoride window were calculated from room-temperature spectral measurements in the 8–12 μm wavelength band using a Digilab Biorad FTS-40 Infrared Spectrometer at Ames Research Center. The appropriate effective optical property is the integrated average product of the surface emittance and the window transmittance. It is weighted with the hemispherical blackbody emissive power per unit wavelength interval over the wavelength range from λ_1 to λ_2, e.g., λ_1=8 μm and λ_2=12 μm , as follows,

$$\varepsilon\tau(T;\lambda_1\lambda_2) = \frac{\int_{\lambda_2}^{\lambda_1} \varepsilon(\lambda,T)\,\tau(\lambda,T)\,e_{\lambda T}\,d\lambda}{\int_{\lambda_1}^{\lambda_2} e_{\lambda T}\,d\lambda} \quad (1)$$

Figure 3 shows the effective emittance of the RCG tile coating calculated using Eq. (1) with the transmittance set to unity to isolate the surface emittance effect. Figure 3 also shows the calculated effective transmittance of the barium fluoride window as a function of window temperature T_w, with the emittance set to unity over the operating range. These predicted values were used as an initial estimate for the radiative properties.

An additional calibration factor F was needed for two reasons. First, the window temperature and temperature gradients cannot be measured with accuracy. Second, there is some uncertainty due to operating outside the range for which the thermographic system was calibrated. Because these effects cannot be unambiguously separated by analysis of the data, both factors are lumped together with the model surface emittance as the effective lumped optical parameter $F\epsilon\tau$ as shown in the last column of Table 1.

As a check on consistency, the lumped parameter was compared qualitatively with the effective properties. The variation of this effective lumped parameter with the surface temperature of the model follows the trend predicted by the effective surface emittance as a function of surface temperature in Fig. 3. The window transmittance variation, shown separately for clarity in Fig. 3, was expected to influence the lumped parameter less strongly because the window temperature T_w was governed by the external flow and cooling, and was not directly coupled to the model surface temperature.

The system was calibrated at the NASA Ames Research Center with the 8–12 μm filter using both a 1300 K blackbody source and a 2300 K blackbody source, as indicated in the second column in Table 1. At that time, it was not possible to calibrate the other filters. The 1300 K blackbody was placed on top of the specimen panel and its cavity aimed vertically toward the scanner. The temperature of the blackbody was then measured with the thermography system using the different filters. In this way, a value was obtained for the combined transmittance of the windows and absorbance of the aluminum mirror for the case where the entire system was at ambient temperature. The calibration factor F in this case equaled one over the calibrated range of temperatures up to 1300 K. The value used for the product of the surface emittance and the window transmittance is valid for temperatures greater than 800 K, since lower surface temperatures are not of interest in this application. Between 1300 and 2300 K the system was calibrated by sighting on a 2300 K blackbody without intervening windows. The thermography system was found to be highly nonlinear in this region. Consequently, a correction curve was generated.

Table 3 Leading-edge temperature rise and the scaled difference between thermocouple and thermographic measurements of the temperature rise at three heat flux conditions

Heat flux, W/cm^2	$T_{C,TC}$ K	$\Delta T_{C,TC}$ K	$\Delta T_{C,TGY}$ K	$\frac{\Delta T_{C,TGY} - \Delta T_{C,TC}}{T_{C,TC}}$
34.6	1608	170	176	0.0037
18.8	1354	33	42	0.0066
7.4	1045	41	36	−0.0048

Table 4 Leading-edge temperature rise vs step height at maximum heat flux condition

	$\Delta T_{C,TGY}$ K	
Steps, mm	Open gaps	Closed gaps
0.25	86	58
0.46	86	38
0.56	129	120
0.76	172	141
0.91	215	184

The effective lumped optical property parameter $F\epsilon\tau$ in the infrared bands transmitted by the other filters appearing in the table exhibits significantly less dependence on the surface temperature, but for different reasons. In the 3–5 μm region, little variation of the room temperature spectral properties was measured, consequently, little variation is expected at the higher temperatures. This is consistent with the relatively slow variation of the lumped emittance-transmittance parameter for the 3–5 μm band. When the 10.6 μm narrowband filter was used, no spectral variation was, of course, possible, and a fixed value of the lumped parameter resulted.

Emittance also varies as a function of observation angle, generally decreasing for dielectrics as the surface becomes parallel with the viewing axis, although this is not a linear relationship. This is not often a problem unless the angle exceeds 45 deg. Particularly when viewed at a glancing angle, the difference in directional emittance is significant. Electromagnetic theory can be used to predict the emittance of a material at a given angle of observation for the two limiting cases of a metal and dielectric.[12] This translates directly into a change in measured radiance, which results in a different apparent temperature. An ideal dielectric surface would appear to be cooler than a metal at the same temperature when viewed at a glancing angle. However, a real surface is not constrained to exhibit these trends, and the directional properties will vary depending on wavelength, surface treatment, surface contamination, and temperature. For example, the directional emittance of titanium shows a behavior similar to a dielectric at one wavelength but similar to a metal at a different wavelength. The angular effects can be corrected for simple geometries using postprocessing by the method described by Balageas et al.[7]

To reduce the effect of angular dependence on the measurements, a mirror was used to bring the measurement angle as close as possible to normal to the surface. The radiative properties are well behaved at normal incidence. In these tests, the only area where the viewing angle exceeded 45 deg was at the edges of the gaps. It was assumed that the emittance follows the theoretical dielectric curve, but no measured data are available. Measurements made at an oblique angle are probably inaccurate, since the radiative properties are not reliably predicted there.

Attempts to image the plasma were unsuccessful, as expected. The effects of the emission, transmission, and absorption by the arc-jet plasma gases are assumed to be negligible. The effect of reflections from the arc is also assumed to be negligible in these tests due to the small angle between the axis of the arc-jet nozzle and the surface of the model. No evidence of reflections from the arc column was observed in these tests.

Results and Discussion

The results of this experiment can be evaluated best by the good agreement between the thermographic temperature measurements, using the lumped effective optical property parameter $F\epsilon\tau$ and temperature measurements made by thermocouples in the same areas on the model.

Figures 4–6 show the temperatures and temperature gradients measured with thermocouples at different locations at the centers of the tiles on the model surface and the temperatures derived from thermographic maps made of the surface. Figures 7–12 are thermographic images of the model during testing. The heated plasma

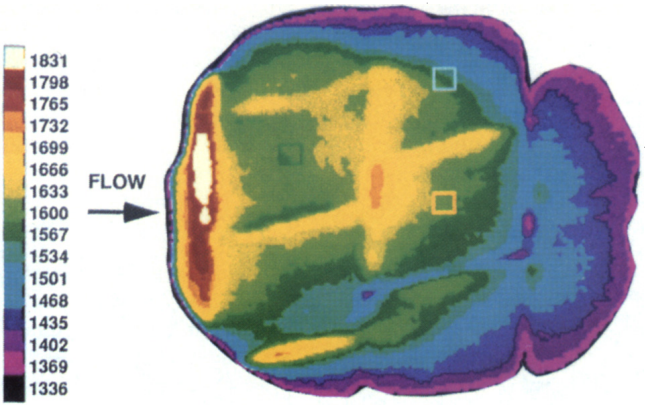

Fig. 7 Infrared image of the test model at the maximum heating condition of 34.6 W/ cm^2, with squares indicating the locations of surface thermocouples.

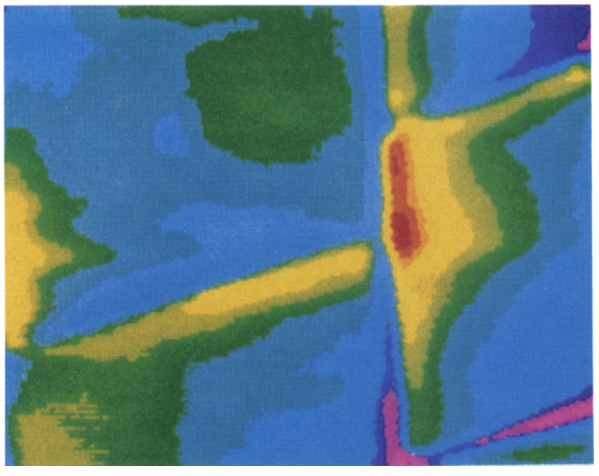

Fig. 8 Close-up at the maximum heating condition.

stream flows from the nozzle on the left to the right. The temperature scale is based on the lumped effective radiative property.

Figures 4 and 5 show the close agreement between the temperatures measured using thermocouples and thermographic monitoring. The temperatures derived from thermocouple measurement and from thermographic monitoring are plotted in Fig. 4 against one another, showing very close agreement for 36 data points corresponding to three points on the surface from different test runs. Very good agreement was obtained between the temperatures from the thermographic data and from surface thermocouples, which were used as a basis for comparison.

The temperature histories for one arc-jet test at one location in the center of the test model were reproduced in detail by the thermographic temperature history as shown in Fig. 5. This test was chosen for the anomalous temperature undershoot before the second heat flux level was established to illustrate how closely the thermographic method tracked the thermocouple measurement of the temperature. The thermographic data are given starting from 90 s, since the lower temperature data were not of interest during the initial transient phase.

Table 2 shows the temperature increases between the center of the top surface on the stepped-up tile and the leading edge as measured by both thermocouples and thermography. The last column in the table shows the ratio of the difference between thermocouple and thermographic measurements of the temperature rise and the absolute value of a characteristic surface temperature at that heating rate. At each of the three heat flux conditions, the difference between the two methods was less than 1% of the absolute temperature. As a result, the thermal gradients visible in the thermographic images of Figs. 7–12 can be used directly with a high degree of confidence to evaluate the temperature rise due to the presence of a step.

Good radiative property data are necessary to calculate the effective emittance and transmittance parameter $\epsilon\tau$ and to predict the trends that the effective optical property parameter will follow. When these radiative property data are insufficient, but reliable temperature data are available, it is possible to calculate a lumped property $F\epsilon\tau$ from the data, but it is impossible to then predict the trend that this lumped parameter will follow or to separate out the different components by calibrations.

The close agreement between the thermocouple data and the ıography data using the lumped effective optical property ıach proves that it is unnecessary to use more than a small ıer of judiciously selected surface points instrumented with mocouples to establish the required optical properties. The ɔed optical property value does not vary across the surface. temperatures derived from the two measurement methods ɛ closely, with a correlation coefficient of 0.95.

ıalyzing pure thermographic temperature data builds on this dation. Having proven that reliable and verifiable agreement s between the two techniques, further experimental data from locations that were not instrumented with thermocouples were analyzed. Figure 6 shows a plot of temperature rise ΔT divided by the absolute temperature of the surface as a function of the tile step height to give a dimensionless quantity for comparison. Table 3 shows the step-height measurement from the adjacent tile to the stepped-up tile and the resulting temperature increases at five loca-

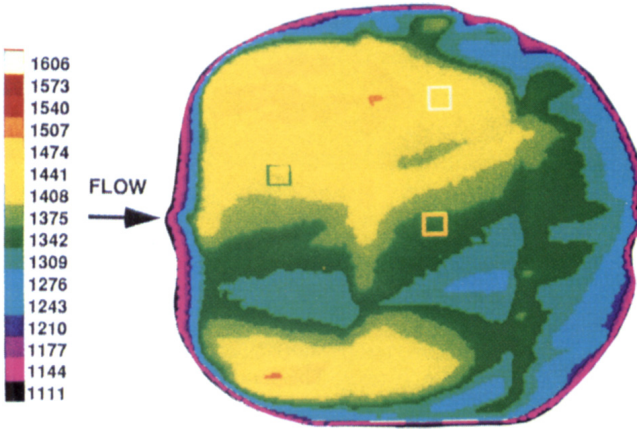

Fig. 9 Infrared image of the test model at the second heating condition of 18.8 W/cm^2.

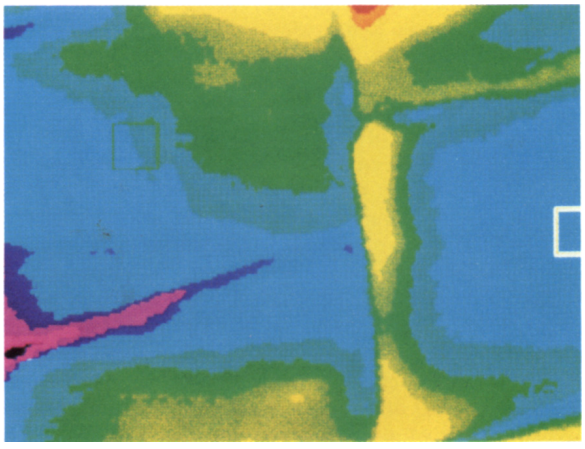

Fig. 10 Close-up at the second heating condition.

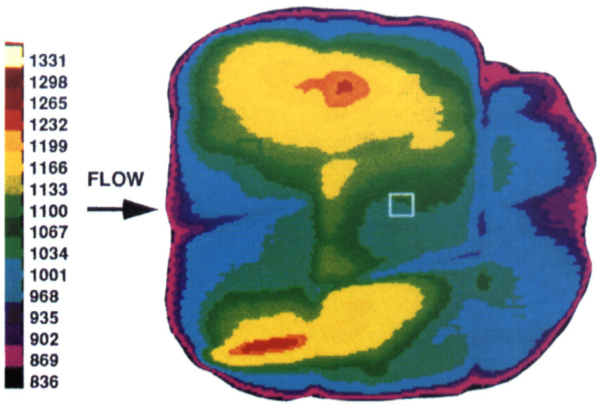

Fig. 11 Infrared image of the test model at the third heating condition of 7.4 W/cm^2.

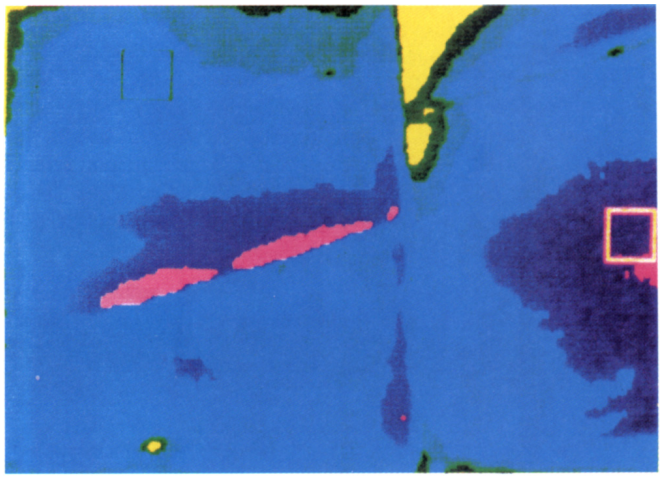

Fig. 12 Close-up at the third heating condition.

tions along the leading edge facing the oncoming flow. Because the tile surfaces were not flat, the steps did not vary linearly along the edge. A representative temperature rise at each of the locations is shown for each of two tests. The temperature increases at the maximum heating rate condition (34.6 W/cm^2) are given in the table. These temperatures were obtained from the thermographic data by subtracting the temperature of an area like those shown in boxes on Fig. 7 on the forward tile from an area on the rearward raised tile. This procedure averages the temperature over an area having a width on the order of a typical surface thermocouple contact length. During the test labeled "open gaps," the gaps between the tiles were left open to the external flow. During the test labeled "closed gaps," these gaps were closed with a high-temperature gap filler material. The gap fillers are used to reduce the flow of hot external gases into and along the gaps.

The absolute values of the tile top surface center thermocouples differed by 21 K between the two tests, reflecting the accuracy of repeatability of the test conditions between the runs. This 21 K represents a 1.3% variation from the tile surface temperature, which is 1600 K. Uncertainties still exist due to the lack of repeatability of external flow conditions between the two tests, possible protrusion of the gap filler, and the effect of conduction down the gap fillers, so the data from both runs were used in the following correlation between the step height and the temperature increase at a stepped-up leading edge normalized by the surface temperature under these external flow and heat transfer conditions. This correlation is shown as a line on Fig. 6:

$$\frac{\Delta T}{T} = 0.1380\Delta X \pm 0.003 \qquad (2)$$

Surface temperature gradients on the model surface are distinctly visible in the thermographic images shown in Figs. 7–12. The center tile in the array was stepped up into the flow by installing a 0.76-mm spacer beneath the tile. The differences between the temperature rises given in the table are much greater than the resolution of the thermographic image, which is 4 K for the 500 K temperature scale spread.

Conclusions

Good agreement between thermocouple and thermographic temperatures has been established using a new approach to calculating the required optical properties under these widely variable arc-jet test conditions. This experimental method can be used with a high degree of confidence to record and store a tremendous amount of surface temperature data in a straightforward and noninvasive manner.

As with any advanced technique, this technique should only be used with a full understanding of its limitations. First, the cost associated with thermographic monitoring greatly exceeds the cost of traditional thermocouple instrumentation. Second, the optical properties vary as a function of observation angle, temperature, and material purity, and appropriate property data are frequently difficult to obtain. The optical property variation can be dealt with using the method described in this paper using a small number of reliable surface temperature measurements. However, the data generated are only as reliable as the thermocouple data on which they are based, although they can be verified to the extent that the material optical properties are known. Finally, the thermographic technique is limited by spatial resolution. To resolve features smaller than the spot size of the standard thermographic setup described in this work, it would be necessary to design an optical system specifically for the desired test configuration.

Conditions for the use of the thermography in these arc-jet tests have not yet been optimized, but plans have been formulated to solve the problems identified. It is expected that, after further development of the techniques, the number of surface thermocouples currently used in arc-jet testing may be reduced to a relatively small number, which would then be used as reference points for thermographic temperature measurements. The thermographic measurements would then assume the role of the primary instrumentation technique.

Acknowledgment

The authors would like to acknowledge the contributions of Domenick Cagliostro of NASA Ames Research Center.

References

[1]Compton, D. L., "Convective Heating Measurements by Means of an Infrared Camera," NASA TM-X 2507, Feb. 1972, pp. 645–660.

[2]Boylan, D. W., Carver, D. B., Stallings, D. W., and Trimmer, L. L., "Measurement and Mapping of Aerodynamic Heating Using a Remote Infrared Scanning Camera in Continuous Flow Wind Tunnels," AIAA Paper 78-799, April 1978.

[3]Bandettini, A., and Peake, D. J., "Diagnosis of Separate Flow Regions on Wind Tunnel Models Using an Infrared Camera," International Congress on Instrumentation in Aerospace Simulation Facilities, Paper 79-171, Monterey, CA, Sept. 1979.

[4]Carlomagno, G. M., DeLuca, L. B., and Lombardi, G., "Characterization of Boundary Layer Conditions in Wind Tunnel Tests Through IR Thermography Imaging," *Proceedings of the Applications of Infrared Technology Meeting* (London, England, UK), Society of Photo-Optical Instrumentation Engineers, Bellingham, WA, June 1988, pp. 23–29.

[5]Monti, R., and Zuppardi, G., "Computerized Thermographic Technique for the Detection of Boundary Layer Separation," *Aerodynamic Data Accuracy and Quality: Requirements and Capabilities in Wind Tunnel Testing*, AGARD N89-16846 09-09, July 1988.

[6]Simeonides, G., Wendt, J. F., Van Lierde, P., Van der Stichele, S., and Capriotti, D., "Infrared Thermography in Blowdown and Intermittent Hypersonic Facilities," *Journal of Thermophysics and Heat Transfer*, Vol. 4, No. 2, 1990, pp. 143–148; see also AIAA Paper 89-0042, Jan. 1989.

[7]Balageas, D., Boscher, D., and Deom, A., "Measurement of Convective Heat Transfer Coefficients on a Wind Tunnel Model by Passive and

Stimulated Infrared Thermography," *Proceedings of the SPIE InfraRed Technology XVI Conference,* (San Diego, CA), Society of Photo-Optical Instrumentation Engineers, Bellingham, WA, July 1990.

[8]Carlomagno, G. M., and DeLuca, L., "Infrared Thermography Applications in Convective Heat Transfer," *Proceedings of the 5th International Symposium on Flow Visualization,* Hemisphere, New York, 1990, pp. 843–848.

[9]Henckels, A., and Maurer, F., "Applications of Infrared Thermography in a Hypersonic Blowdown Wind Tunnel," *Proceedings of the 13th International Congress on Instrumentation in Aerospace Simulation Facilities,* Institute of Electrical and Electronics Engineers, New York, 1989, pp. 516–524.

[10]Hube, F. K., "Simulated Thermal Protection Tile Roughness Effects on Windward Surface Heat Transfer on the Rockwell International Space Shuttle Orbiter," Arnold Engineering Development Center, Rept. A034-733, Arnold Air Force Station, TN, Jan. 1977.

[11]Neiland, V. Y., "The Convergence of the Orbiter 'Buran' Flight Test and Preflight Study Results, and the Choice of a Strategy to Develop a Second Generation Orbiter," AIAA Paper 89-5019, July 1989.

[12]Siegel, R., and Howell, J. R., *Thermal Radiation Heat Transfer,* 2nd ed., McGraw-Hill, New York, 1981, pp. 101–117.

Ronald K. Clark
Associate Editor